

Gem-quality Green Cryptocrystalline Muscovite (Fuchsite) from Ya'an Prefecture, Sichuan, China

Féodor Blumentritt, Franck Notari, Marion Becouze, Maxence Vigier, Guillaume Zuber, Candice Caplan and Emmanuel Fritsch

ABSTRACT: An attractive massive green gem material from central China was recently purchased by the authors as 'chrome-pyrophyllite', but proved to be cryptocrystalline Cr-bearing muscovite (fuchsite). The material contains inclusions of ochrous rutile, tourmaline needles, granular quartz, black masses of disordered graphite, and pyrite that is locally altered to black hematite and brownish red lepidocrocite. EDXRF chemical analysis showed the expected major constituents Al, Si and K, as well as minor-to-trace amounts of S, Ba, Ti, Cl, Fe, Cr, V, Rb, Mn and Mg (some of which may be due to inclusions). UV-Vis-NIR spectroscopy showed that the green colour of the muscovite is due to Cr³⁺ and V³⁺. The material exhibits whitish blue fluorescence to long-wave UV radiation as well as blue persistent luminescence—neither of which has been documented previously in muscovite—and these features are tentatively assumed to be associated with oxygen vacancies. This new material from China is similar to massive fuchsite from Ethiopia and Myanmar.

The Journal of Gemmology, 39(1), 2024, pp. 66–76, <https://doi.org/10.15506/JoG.2024.39.1.66>
© 2024 Gem-A (The Gemmological Association of Great Britain)

In June 2022, the authors encountered some rough, pebble-shaped green stones being sold on eBay.com as chrome-pyrophyllite from Ya'an Prefecture in China's Sichuan Province (e.g. Figure 1). We were impressed by the homogeneity of this material and its attractive bright green to deep green colour in transmitted light. Initial observations suggested its homogeneity was due to a cryptocrystalline texture consisting of minute grains not visible with an optical microscope (i.e. up to approximately 160×).

We performed a search for similar-looking items in the gemmological literature and on the internet, and found only one instance of a material described as chrome-pyrophyllite from the same reported Ya'an locality (<https://www.mindat.org/loc-145501.html>, accessed 4 August 2023). In addition, a green rock with a similar cryptocrystalline texture and colour is known as *chromocre* (N. Meisser, pers. comm. 2023; Figure 2) and comes from Ecouchet, Autun,

Saône-et-Loire department, France. *Chromocre* has also been identified as pyrophyllite (Kiefer 1953). Thus, based only on visual comparisons to similar material, the samples we procured were likely chrome-pyrophyllite. Nevertheless, Raman spectroscopic analyses identified the material as muscovite.

The aim of this article is to characterise this gem-quality green cryptocrystalline muscovite from China. We describe its gemmological, structural and chemical characteristics, and also document its unexpected blue luminescence. Moreover, in the absence of information on its geological occurrence, we make some assumptions about its formation based on its inclusions and associated minerals.

MATERIALS AND METHODS

For this study, we obtained from a Chinese dealer (via eBay.com) about 100 rough samples ranging from approximately 3 to 15 g. The pieces had been

Figure 1: Cryptocrystalline muscovite (fuchsite) has recently appeared on the market as 'chrome-pyrophyllite' from Ya'an Prefecture, Sichuan, China. The rectangular sample polished on two sides shown at the centre is approximately 2.7 cm high. Photo by F. Blumentritt.



slightly impregnated with oil to better show off their colour. We selected about 35 rough samples that were relatively free of inclusions and cut several cabochons for this study (e.g. Figures 1 and 3). These cabochons weighed between 1.48 and 10.73 ct, with most of them around 2–4 ct.

For comparison, we examined a 1.42 ct cabochon



Figure 2: Chromocre (Cr-bearing pyrophyllite) from France may resemble the new material from China. Photo courtesy of Nicolas Meisser.

of fuchsite from Myanmar that was purchased at a gem show; it had a light green colour similar to some of the samples from China (Figure 3). In addition, we studied a 6.82 ct faceted fuchsite from Ethiopia that was obtained from T. Pradat (Gem-Plus, Paris, France). Such material was initially sold as emerald, but can be readily identified by its gemmological properties (Pradat *et al.* 2013). The sample had a similar texture as the Chinese material, but its green



Figure 3: Some of the samples examined for this study include: (1) a 1.42 ct fuchsite cabochon from Myanmar; (2) a 6.82 ct faceted fuchsite from Ethiopia; and (3) a selection of cryptocrystalline muscovite cabochons from China (here, oiled with paraffin). The cabochon in the front weighs 8.39 ct. Photo by F. Blumentritt.

colour was lighter and more yellowish (again, see Figure 3).

RI and SG values were measured on ten cabochons from China (with a fairly flat surface), and on both samples from Ethiopia and Myanmar, using a Gem-A Instruments refractometer and a Mettler AE 1000 C hydrostatic balance, respectively. The optical behaviour of all analysed samples was observed with a Leica M125 microscope using diffused cross-polarised light. Hardness was tested with an in-house Mohs hardness pencil kit on a dozen polished samples (either cabochons or those polished for chemical analysis). Luminescence was observed while exposed to long- and short-wave UV radiation and a 405 nm laser. Photomicrographs of inclusions and impurities in the muscovite were taken using a Leica M205 binocular microscope with z-stack capability and a DMC5400 camera.

The low hardness of muscovite (about 2½ on the Mohs scale) and its perfect cleavage usually make it unsuitable for jewellery purposes. However, the cryptocrystalline texture of the material from China increases the toughness (tenacity) of the material, which can be easily cut and polished. The surfaces of our cabochons commonly had small fractures that created cloudy whitish patches, so we conducted impregnation experiments on 12 of the cabochons using cedarwood oil and mineral oil (liquid paraffin) to check their effectiveness for masking surface blemishes.

Raman spectra of about 30 rough and polished green muscovite samples, and their inclusions and associated minerals, were acquired using a Thermo Scientific DXR3 Raman microscope equipped with 532 nm laser excitation (10 mW) in the range between 50 and 3570 cm⁻¹.

Powder X-ray diffraction (XRD) was performed on one sample chosen for its apparent low content of inclusions. The specimen was crushed in an agate mortar for 10 minutes to maximise the homogeneity of grain sizes. XRD patterns were collected at room temperature with a Bruker D8 Advance diffractometer using monochromatic Cu K-L₃ ($\lambda = 1.540598 \text{ \AA}$) X-rays and a LynxEye detector.

Chemical analyses were conducted with a Thermo Scientific ARL Quant'X energy-dispersive X-ray fluorescence (EDXRF) spectrometer equipped with an Rh X-ray tube for excitation and a Peltier-cooled silicon drift detector. Each spectrum was accumulated over 300 s for the six filters, and a rotating sample holder made it possible to average the analysis over a selected 2-mm-diameter area. The size of the analysed spot did not permit measurement of the muscovite alone, but

probably also encompassed inclusions, despite the selection of relatively pure samples through microscopic observation. Analyses were initially obtained on 12 samples of the muscovite to identify elements detectable by EDXRF spectroscopy, as this technique is not capable of quantifying elements lighter than Na. However, EDXRF analyses can measure most of the elements expected in muscovite and also provide a fair estimate of concentration for the major components Al, Si and K. Additional elements were included in our semi-quantitative method by noting those documented in the chemical analyses of muscovite in the literature (Brigatti *et al.* 2001a, b; Antohi-Trandafir *et al.* 2018; Pirouei *et al.* 2020). Finally, we obtained semi-quantitative EDXRF analyses for 20 samples that were polished on one side.

Ultraviolet-visible-near infrared (UV-Vis-NIR) transmission spectra were acquired on ten cabochons in the 300–1050 nm range using a custom-made four-channel spectrometer equipped with three Peltier-cooled CCD detectors. Absorption spectra were first collected at room temperature, but some weak features were observed that required us to re-acquire the spectra under low-temperature conditions (77 K) for better resolution; the positions of the absorption maxima should not be affected by temperature.

Following the observation of whitish blue luminescence under long-wave UV radiation and the 405 nm laser, luminescence spectroscopy was performed on ten rough samples and ten cabochons. We used a GGTL Laboratories DFI V3R system operated with a high-intensity UV lamp (xenon 300 W) and a 405 ± 0.2 nm laser with a power of 200 mW. Spectra were acquired at low temperature (77 K). The samples were first cleaned with acetone to suppress any possible influence of oil residues on the luminescence (cf. Notari *et al.* 2002, 2022). Spectral decomposition was performed for five of the luminescence spectra acquired from the 20 samples (all of which had the same features). The spectra were recast on an energy (eV) scale, and spectroscopic features were decomposed with an acceptable minimum of Gaussian functions using a least-squares approach for fit. The electronic transitions were simulated in an energy-level distribution related to the Boltzmann function (Atkins & de Paula 2006). The peak parameters (position, intensity and full width at half maximum [FWHM]) were unrestricted during the fitting until the position remained consistent with the analysed spectra. The peak position was then fixed while the FWHM and intensity remained unrestricted.

RESULTS

Gemmological Properties and Impregnation Testing

The gemmological characteristics of the Chinese samples are summarised in Table I. In reflected light, the specimens appeared light to dark green with slight yellowish or bluish variations. In transmitted light, they appeared vivid green. The material consisted of agglomerated grains, yielding an aggregate polariscope reaction. Individual grains could not be seen with the optical microscope, and thus we considered them to be of micrometric size, giving the overall cryptocrystalline texture. In rare samples, larger grains (about 500 µm measured with the microscope) were encountered. In such cases, grains easily flaked off the sample simply by handling it. Exposure to 365 nm long-wave UV radiation—and to 405 nm laser excitation—caused the samples to exhibit a moderate to bright whitish blue luminescence (e.g. Figure 4). A similar luminescence colour was emitted by the Ethiopian and Burmese samples.

The Ethiopian fuchsite had gemmological characteristics that were consistent with those obtained from our Chinese samples. The only significant difference was that its SG fell in the range of 2.80–2.90, as reported by Prada *et al.* (2013), which is higher than the 2.76–2.85 range obtained for the Chinese material, but this could be due to the influence of mineral inclusions or porosity. The SG of the sample from Myanmar (2.83) was within the range we obtained for the material from China.

Impregnation testing was initially done with organic oil (thick cedarwood oil used for emeralds) under a pressure of about 900 bars at 60°C for 48–72 h, but the experiments were unsuccessful due to the oil gradually seeping out of the fractures. The use of mineral oil under the same conditions yielded stable results, at least since the experiment was performed in December 2022. The mineral oil effectively masked surface blemishes on the cabochons, which had an appearance sometimes resembling attractive green jade (again, see Figure 3).

Table I: Gemmological characteristics of the green cryptocrystalline muscovite from China.

Property	Description/value
Colour	Light to dark slightly yellowish or slightly bluish green
Optical behaviour	Aggregate
Transparency	Translucent to near opaque
Lustre	Greasy, silky to sub-vitreous
Cleavage	None seen
Hardness	Mohs 2½
RI (spot)	1.56–1.57
SG	2.76–2.85

Inclusions and Associated Minerals

Microscopic observations revealed various impurities in the Chinese samples (Figures 5–7). Most of the rough stones contained relatively large patches of ochrous yellow to orange yellow material (Figure 5a), which was identified by Raman spectroscopy as rutile, consistent with the relatively high concentration of Ti in all the specimens (see chemical analyses below). Some rough samples contained small cavities hosting blue azurite crystals (Figure 5b). In addition, colourless to dark yellowish green, acicular inclusions were identified by Raman spectroscopy as tourmaline in at least three of the 30 analysed samples (Figure 5c), although the specific species of the tourmaline group could not be determined. At the interface with the rock matrix, some colourless granular quartz inclusions occurred in the muscovite (Figure 5d). In one sample, we recorded a Raman spectrum corresponding to orpiment (As₂S₃), but we were unable to obtain a good photomicrograph due to its small size.

Millimetre-size crystals of pyrite were easily visible on the surface of some rough samples, especially in the matrix, and were sometimes embedded in the muscovite as inclusions (Figure 6). Most of these embedded pyrites were partially altered along the interface with the host muscovite by oxidation into black hematite (Fe₂O₃) and brownish red lepidocrocite [FeO(OH)], as identified by Raman spectroscopy.



Figure 4: Two samples of rough cryptocrystalline muscovite from China are shown in ambient light (left) and emitting whitish blue luminescence while being exposed to 365 nm long-wave UV radiation (right). The lighter coloured sample on the left (1.58 g) fluoresces brighter than the darker specimen on the right (1.06 g). Photos by F. Blumentritt.

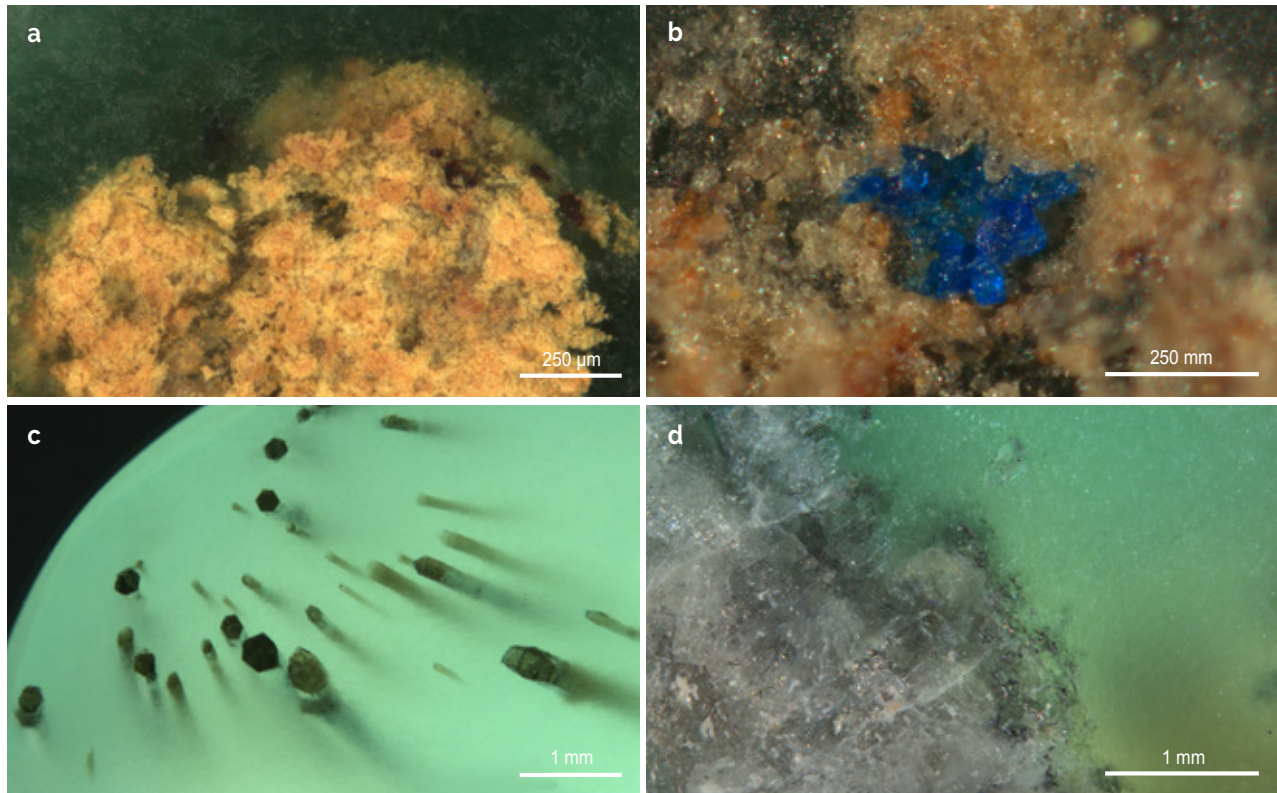


Figure 5: Impurities observed in the cryptocrystalline muscovite from China include (a) ochrous yellow-orange rutile, (b) azurite in minute cavities, (c) dark green tourmaline and (d) quartz. Photomicrographs by F. Notari.

Some samples contained cloudy aggregates of minute black inclusions surrounding muscovite grains (Figure 7). Their Raman spectra indicated an amorphous structure, with two broad bands centred at about 1350 and 1600 cm^{-1} , which best correspond to the D and G peaks, respectively, of disordered graphite (cf. Ferrari & Robertson 2000; Zhang *et al.* 2019).

Dolomite and calcite were identified in areas of matrix material surrounding the muscovite.

Structural Characterisation

XRD analysis of a powdered sample confirmed the atomic structure of muscovite. Two structural polytypes of muscovite (i.e. rotation of successive atomic layers along the *c*-axis) are known as 1M (without rotation) and 2M₁ (successive rotations of +120° and -120°; Nespolo 2001). The analysed sample belongs to the *C2/c* space group and is thus related to the 2M₁ polytype, characteristic of a metamorphic genesis (Deer *et al.* 1992). Structural

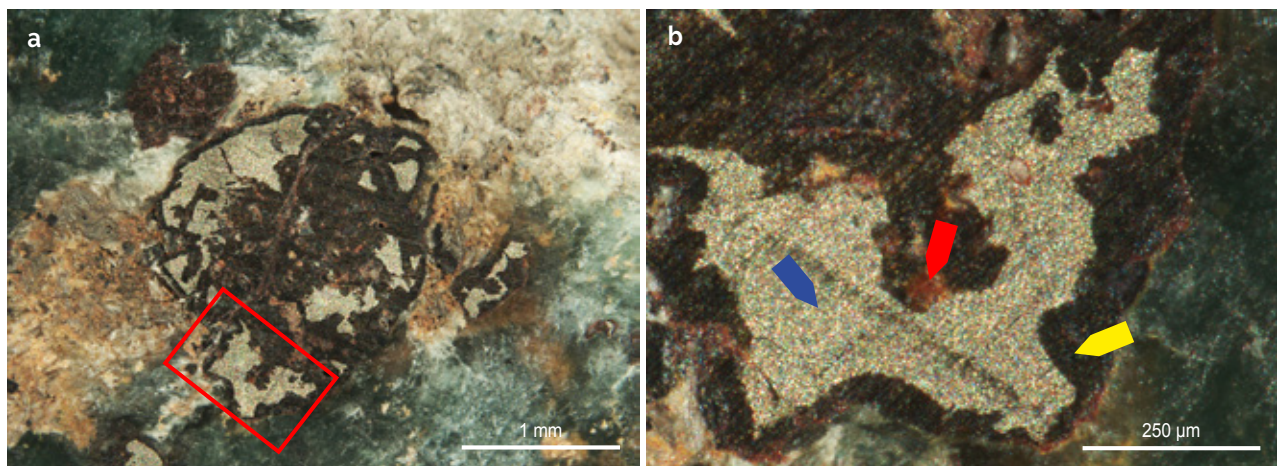


Figure 6: (a) Pyrite inclusions in the cryptocrystalline muscovite show alteration features. (b) A detail of the area in the red rectangle reveals pyrite (blue arrow), lepidocrocite (red arrow) and hematite (yellow arrow). Photomicrographs by F. Blumentritt.

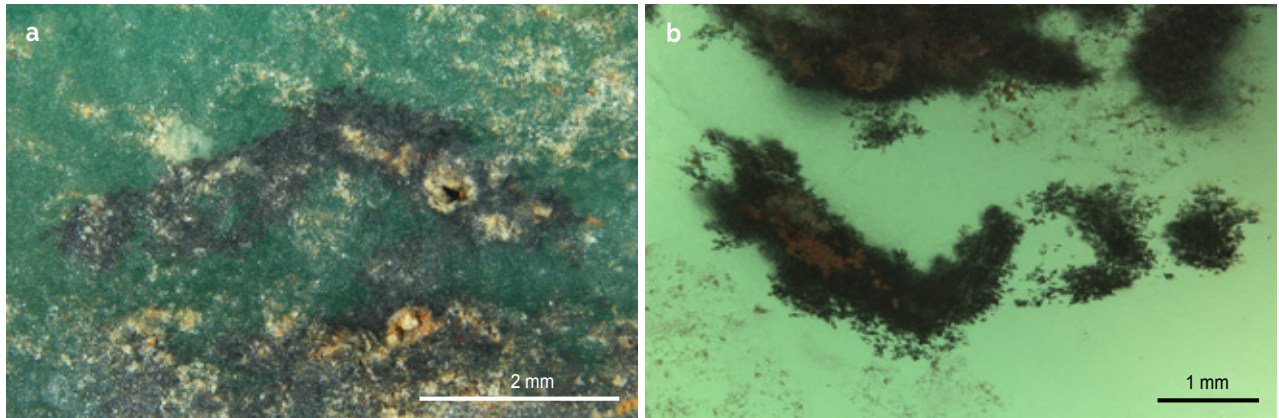


Figure 7: Patches of black inclusions in the cryptocrystalline muscovite were identified as disordered graphite, and are shown here in (a) reflected light and (b) transmitted light. Photomicrographs by F. Notari.

parameters calculated from the Rietveld refinement of a diffractogram are shown in Table II. This refinement takes into account a preferential orientation artefact in the {001} plane that is typical of the mica group.

Crystallite size can be estimated from the Rietveld refinement because it is related to the FWHM of the diffraction peaks. The calculated size is less than 1 μm , consistent with the cryptocrystalline texture inferred from microscopic observation.

Chemical Composition

EDXRF data for the 20 Chinese samples that were analysed using our semi-quantitative technique showed that four specimens had lower concentrations of K and higher values of Ca, Si, Fe and S, in variable proportions, than the expected values for muscovite. These anomalies were probably due to inclusions such as dolomite ($\text{CaMg}[\text{CO}_3]_2$), quartz (SiO_2) and pyrite (FeS_2), all three of which were identified in various samples in this study by Raman spectroscopy. The remaining 16 specimens showed major amounts of Al, Si and K (see the semi-quantitative data in Table III), as would be

expected for the main constituent elements of muscovite. Using the average values of these elements (and also Na) for these 16 samples, we calculated a structural formula

Table III: EDXRF semi-quantitative chemical analyses of the green cryptocrystalline muscovite from China.

Component	Range	Average
Major elements (wt.%)		
Al_2O_3	35.2–39.2	38.5
SiO_2	40.4–46.3	40.4
K_2O	9.6–16.0	13.0
Minor and trace elements (ppmw)		
Na	4200–26200	10000 \pm 500
Mg	720–3590	260 \pm 90
S	5880–10570	7310 \pm 60
Cl	2500–9300	4200 \pm 200
Ca	bdl–7434	856 \pm 8
Sc	11–74	19 \pm 1
Ti	160–48580	4950 \pm 20
V	130–3360	1520 \pm 10
Cr	bdl*–5300	2130 \pm 20
Mn	20–545	292 \pm 7
Fe	3–10780	2810 \pm 10
Co	bdl	bdl
Ni	bdl–60	24 \pm 2
Ga	bdl–320	168 \pm 3
Br	bdl–2.5	0.6 \pm 0.2
Rb	1–2195	1009 \pm 4
Sr	bdl–1560	285 \pm 3
I	bdl–150	50 \pm 20
Cs	bdl–240	50 \pm 20
Ba	bdl–11100	5500 \pm 300
Eu	bdl–0.44	0.05 \pm 0.01

* Abbreviation: bdl = below detection limit.

Table II: Structural parameters of the Chinese green cryptocrystalline muscovite calculated from XRD refinement.

Parameter	Value
Space group	$C2/c$
Z	2
a	5.1859(6) \AA
b	8.9989(9) \AA
c	20.108(2) \AA
α	90°
β	95.779°
γ	90°
Calculated crystallite size	<1 μm
Calculated density	2.81 g/cm^3

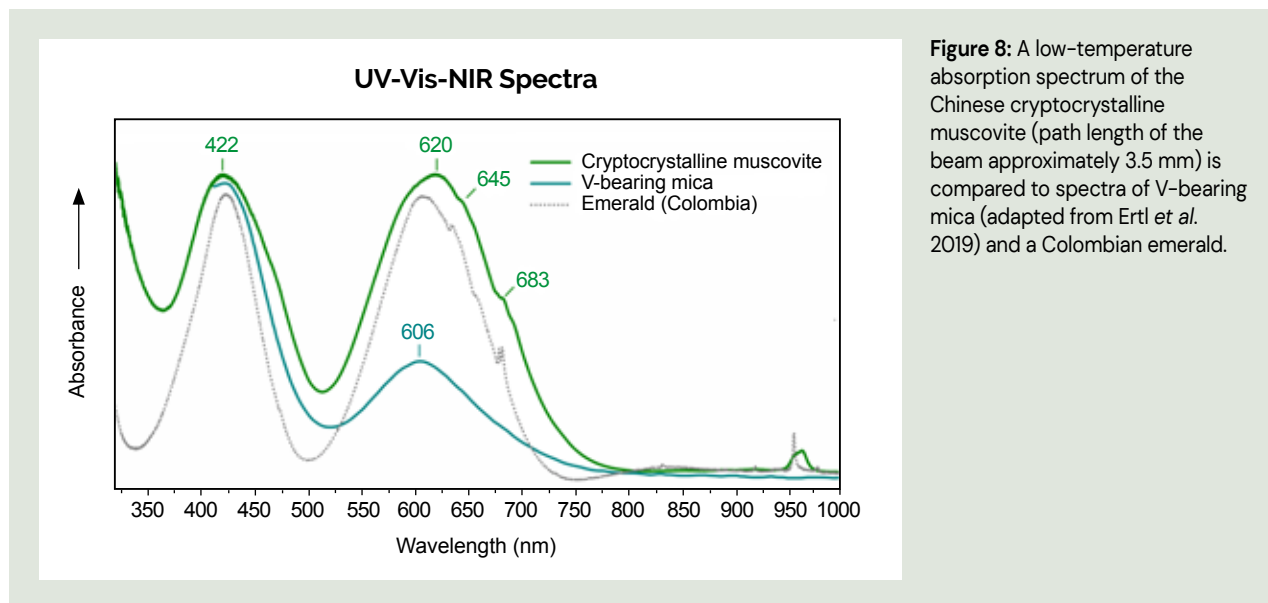


Figure 8: A low-temperature absorption spectrum of the Chinese cryptocrystalline muscovite (path length of the beam approximately 3.5 mm) is compared to spectra of V-bearing mica (adapted from Ertl *et al.* 2019) and a Colombian emerald.

close to the ideal formula of muscovite: $(\text{Na}_{0.1}\text{K}_{1.1})\text{Al}_{1.9}(\text{Al}_{1.1}\text{Si}_{2.9}\text{O}_{10})(\text{OH})_2$.

Noticeable amounts of S, Ba, Ti, Cl, Fe, Cr, V, Rb, Mn and Mg were also measured. However, we did not include these elements in the structural formula because of the semi-quantitative nature of the EDXRF analysis and the possibility that some of them are due to inclusions.

The samples from Ethiopia and Myanmar yielded similar chemical data, except that both had much greater Ba (about 3–5 times higher) than the Chinese specimens. Additional chemical analyses are required to confirm whether Ba concentration could be useful to separate the Chinese material from these other localities.

UV-Vis-NIR Spectroscopy

Previous spectroscopic analysis of material from Ethiopia (Pradat *et al.* 2013) determined that Cr was responsible for the green colour. Low-temperature UV-Vis-NIR spectra recorded for the Chinese samples confirmed the main influence of Cr on their colour (Figure 8), consistent with the presence of this element that was measured by EDXRF. The spectral features are very similar to those of emerald (grey dotted trace in Figure 8, from a GGTL reference specimen), and appear to result from a mixture of absorptions due to Cr^{3+} (Faye 1968; Reddy *et al.* 2003; Pradat *et al.* 2013) and V^{3+} (Ertl *et al.* 2019; blue trace in Figure 8). The influence of V^{3+} on the spectrum of the Chinese muscovite is seen by a slight shift of the transmission window towards higher wavelengths when compared to a spectrum for only Cr^{3+} in mica (at about 520 nm; see GRR 1461 at <http://minerals.gps.caltech.edu/files/visible/mica/index.html>). This is consistent with

the presence of both Cr (average 2130 ppm) and V (average 1520 ppm) in our samples. The weak features between 640 and 700 nm are due to Cr^{3+} -forbidden transitions (see, e.g., Wood & Nassau 1968). No Fe^{3+} features appear to be present.

Luminescence Spectroscopy

Low-temperature luminescence spectroscopy of the Chinese samples showed typical features of Cr^{3+} in octahedral coordination, such as a sharp band at 690 nm (as documented in Cr-bearing clinocllore; Czaja *et al.* 2014), a broad band centred at about 760 nm, and a large asymmetric band with an apparent maximum just below 500 nm at the very end of the blue region (Figure 9). The position of this maximum explains the blue colour of the luminescence, and its width—covering the entire visible range—is responsible for the whitish appearance. This spectrum is consistent with those recorded for our two samples from Ethiopia and Myanmar under the same conditions. The large feature centred at about 760 nm could be a side band of the chromium *R*-lines (Han *et al.* 2020), as seen in emerald.

The asymmetric shape of the band at about 500 nm (Figure 9, red trace) suggests the presence of overlapping contributions. To the authors' knowledge, blue luminescence of fuchsite to long-wave UV radiation has not been previously documented, so only comparisons with other materials are possible here. Decomposition of the 500 nm feature revealed five possible bands at 467, 497, 525, 558 and 609 nm (again, see Figure 9). This illustrates the complexity of this emission and eliminates certain possibilities that typically induce a single large, essentially symmetric

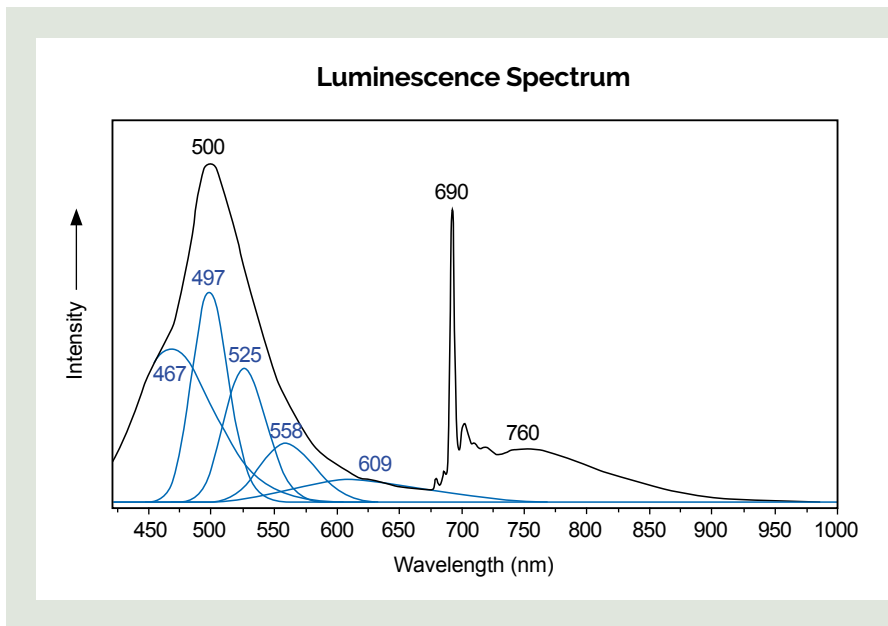


Figure 9: A low-temperature luminescence spectrum of the Chinese cryptocrystalline muscovite obtained with 405 nm excitation shows Cr³⁺-related bands at 690 and 760 nm, and a broad, asymmetric feature with a maximum around 500 nm that is likely associated with the observed whitish blue luminescence. A proposed decomposition of the 500 nm band reveals several peaks at 467, 497, 525, 558 and 609 nm (blue traces).

band, such as Eu²⁺ emission (Gaft *et al.* 2015). The 500 nm emission also does not correspond to blue emission from any of the inclusions or associated materials we documented. Furthermore, chemical analysis revealed no obvious candidate as an activator of this luminescence. Similar complex blue emission characterised by a broad band at about 500 nm in response to long-wave UV has been documented for simple oxides such as ZnO (Sambandam *et al.* 2015), ZrO₂ (Wang *et al.* 2021) and MgO (Summers *et al.* 1983), and even for some simple silicates (e.g. in opal; Gaillou *et al.* 2008). In these binary materials (ZnO, ZrO₂, MgO, etc.), the blue luminescence has been attributed to oxygen vacancies, an intrinsic defect possibly not related to any particular impurity. Oxygen vacancies are probably the most common defect in oxides, but they are difficult to identify unequivocally. Thus, we suggest—speculatively, as there is no proof—that the particular emission described here could be due to such intrinsic oxygen vacancy defects.

In some samples, we also noticed a persistent blue luminescence (commonly but inaccurately referred to as ‘phosphorescence’) that was visible for a few seconds after the laser was turned off. Similar luminescence has been documented in MgO containing oxygen vacancies (Summers *et al.* 1983), which could also partially support the role of oxygen vacancies in the blue luminescence of this muscovite.

ANOTHER MUSCOVITE VARIETY?

To date, more than 30 varieties of muscovite have been reported (Rieder *et al.* 1999; Melka 2009), mainly associated with variations in chemical composition,

but also in colour, structure or habit.

Based on gemmological considerations, the Chinese material studied for this article might be referred to as ‘batchelorite’, a slightly Cr-bearing muscovite from Tasmania. Although this variety has been described as ‘slaty’ (Petterd 1910), the only photograph in Mindat (<https://www.mindat.org/min-566.html>, accessed 8 August 2023) shows a sample very similar to the material analysed here. However, the chemical formula for batchelorite given by Bothwell & Moss (1957) lacks the relatively high content of Cl that was measured in our samples (see Table III). Thus, although they are close in appearance, we prefer not to use ‘batchelorite’ when referring to the material from China.

Some varieties of muscovite belong to one specific structural polytype of this material. However, since the polytype has not been defined systematically for all muscovite varieties, this consideration is unfortunately not useful for determining a possible variety name for this material. Muscovite varieties can also be defined based on chemical considerations. According to the concentrations obtained from our EDXRF analysis, one could consider this material to be a Ti-rich variety, for example, assuming that Ti is included in the muscovite and is not present only as the rutile impurities identified by Raman spectroscopy. However, the presence of high concentrations of other elements such as Ba, Cl, Fe, Cr, V, Rb, Mn and Mg cannot be ignored. Hence, this material should not be considered as a specific element-rich variety of muscovite.

Spectroscopic analyses highlight the role of Cr and V as the main chromophores responsible for the green colour. Among Cr-bearing mica, two varieties of

muscovite could correspond to the material analysed here: fuchsite and mariposite (Whitmore *et al.* 1946). Mariposite, with the ideal structural formula $K(Al,Cr)_2(Al,Si)_4O_{10}(OH)_2$, is defined in the literature to be closest in composition to phengite, a Si-rich mica series (3.1–3.5 Si per formula unit; Tappert *et al.* 2013). Since the calculated structural formula of the Chinese material indicates Si < 3, this material is unlikely to be mariposite. Thus, as was previously proposed for similar material from Ethiopia (Pradat *et al.* 2013)—and based on our structural, chemical and spectroscopic results—we can reasonably identify this material as cryptocrystalline fuchsite.

GEOLOGICAL CONTEXT

Raman spectroscopy revealed that the matrix material hosting the cryptocrystalline fuchsite is mainly formed by fine-grained dolomite with some quartz and calcite—thus a dolomitic rock or dolostone (Friedman & Sanders 1967). The formation of gem-quality fuchsite in this rock probably resulted from a complex series of processes, according to the geological history of the Ya'an region.

Ya'an Prefecture is located in the Sichuan fold-thrust belt, in the south-western Sichuan foreland basin. During its evolution, the Sichuan basin experienced multiple tectonic cycles that include the Guangxi (Caledonian), the Yunnan and Dongwu (Hercynian), the Indosinian, the Yanshanian and the Himalayan events, resulting in multiple regional unconformities and rock denudation processes (Wang *et al.* 1989). The region initially experienced a rifting period, followed by a carbonate platform depositional environment from

the Permian to Middle Triassic (Ryder *et al.* 1994). Subsequently, pervasive dolomitisation and cementation of carbonates formed coarsely crystalline dolomites, some of which have high porosity (Yang *et al.* 2019). Dolomitisation could have been locally facilitated by high temperatures associated with volcanism in the area, or volcanic-related dolomitising fluids (e.g. Jiang *et al.* 2017; Zheng *et al.* 2019; Chen *et al.* 2020). Then, several orogenic phases linked to the collision of the Yangtze platform with eastern Tibet (Indosinian orogeny) led to a flexural subsidence, forming the foreland basin in the Late Triassic that filled with continental sediments (Mu *et al.* 2019). During this burial process, the sediments expelled large amounts of fluids, which could have facilitated muscovite precipitation in the dolomite that was deposited during the carbonate platform phase. These formations outcrop today in the Ya'an region (Chen *et al.* 2020).

The presence of graphitic carbon-related inclusions in the fuchsite could be related to the compressional tectonics that drove a flow of basinal fluids associated with hydrocarbons that are also present in this basin (Hu *et al.* 2023). These disordered graphitic inclusions could also explain the presence of relatively high amounts of V in the fuchsite, since buried organic materials commonly contain this element (Olivier 2006). The presence of azurite in small cavities within the fuchsite is consistent with a later metamorphic process accompanied by oxidising hydrothermal fluids at low pressure and low temperature (Melchiorre *et al.* 2000). The alteration of pyrite into hematite and lepidocrocite suggests that these conditions could have continued after the precipitation of the cryptocrystalline muscovite.

CONCLUSION

A detailed characterisation of what was initially presented as gem-quality chrome-pyrophyllite identified the material as green cryptocrystalline muscovite (fuchsite). The cryptocrystalline texture (which increases the material's toughness) and its attractive appearance make it suitable for some jewellery purposes (i.e. set in pendants, earrings, brooches, etc.; e.g. Figure 10). The genesis of this muscovite could be related to a multistep process involving metamorphism, hydrothermal activity and metasomatism.

To the best of the authors' knowledge, blue luminescence has not been previously documented for natural muscovite. The involvement of oxygen vacancies in this emission is one possibility, consistent with our data, but further research is necessary to definitively prove the cause.



Figure 10: A cabochon of cryptocrystalline muscovite from China (about 5 ct) is set in a pendant to illustrate the potential use of this material in jewellery. Photo G. Zuber.

REFERENCES

- Antoхи-Trandafir, O., Timar-Gabor, A., Vulpoi, A., Bălc, R., Longman, J., Veres, D. & Simon, S. 2018. Luminescence properties of natural muscovite relevant to optical dating of contaminated quartz samples. *Radiation Measurements*, **109**, 1–7, <https://doi.org/10.1016/j.radmeas.2017.12.004>.
- Atkins, P. & de Paula, J. 2006. *Physical Chemistry*, 8th edn. Oxford University Press, Oxford, 1,072 pp. (see pp. 436–437).
- Bothwell, D.I. & Moss, A.A. 1957. The nature of batchelorite. *Mineralogical Magazine and Journal of the Mineralogical Society*, **31**(239), 700, <https://doi.org/10.1180/minmag.1957.31.239.09>.
- Brigatti, M.F., Galli, E., Medici, L., Poppi, L., Cibin, G., Marcelli, A. & Mottana, A. 2001a. Chromium-containing muscovite: Crystal chemistry and XANES spectroscopy. *European Journal of Mineralogy*, **13**(2), 377–389, <https://doi.org/10.1127/0935-1221/01/0013-0377>.
- Brigatti, M.F., Kile, D.E. & Poppi, M. 2001b. Crystal structure and crystal chemistry of lithium-bearing muscovite-2M₁. *Canadian Mineralogist*, **39**(4), 1171–1180, <https://doi.org/10.2113/gscanmin.39.4.1171>.
- Chen, H., Zhu, M., Chen, S., Xiao, A., Jia, D. & Yang, G. 2020. Basin-orogen patterns and the Late Triassic foreland basin conversion process in the western Yangtze block, China. *Journal of Asian Earth Sciences*, **194**, article 104311, <https://doi.org/10.1016/j.jseas.2020.104311>.
- Czaja, M., Kądziołka-Gaweł, M., Lisiecki, R., Bodył-Gajowska, S. & Mazurak, Z. 2014. Luminescence and other spectroscopic properties of purple and green Cr-clinochlore. *Physics and Chemistry of Minerals*, **41**(2), 115–126, <https://doi.org/10.1007/s00269-013-0629-x>.
- Deer, W.A., Howie, R.A., & Zussman, J. 1992. *An Introduction to the Rock-Forming Minerals*, 2nd edn. Longman Scientific & Technical, Essex, 696 pp. (see pp. 288–293).
- Ertl, A., Rakovan, J., Hughes, J.M., Bernhardt, H.-J. & Rossman, G.R. 2019. Vanadium-rich muscovite from Austria: Crystal structure, chemical analysis, and spectroscopic investigations. *Canadian Mineralogist*, **57**(3), 383–389, <https://doi.org/10.3749/canmin.1900020>.
- Faye, G.H. 1968. The optical absorption spectra of certain transition metal ions in muscovite, lepidolite, and fuchsite. *Canadian Journal of Earth Sciences*, **5**(1), 31–38, <https://doi.org/10.1139/e68-003>.
- Ferrari, A.C. & Robertson, J. 2000. Interpretation of Raman spectra of disordered and amorphous carbon. *Physical Review B*, **61**(20), 14095–14107, <https://doi.org/10.1103/PhysRevB.61.14095>.
- Friedman, G.M. & Sanders, J.E. 1967. Chapter 6: Origin and occurrence of dolostones. In: Chilingar, G.V., Bissell, H.J. & Fairbridge, R.W. (eds) *Carbonate Rocks: Origin, Occurrence and Classification*. Elsevier, Amsterdam, The Netherlands, Developments in Sedimentology **9A**, 267–348, [https://doi.org/10.1016/s0070-4571\(08\)71114-2](https://doi.org/10.1016/s0070-4571(08)71114-2).
- Gaft, M., Reisfeld, R. & Panczer, G. 2015. *Modern Luminescence Spectroscopy of Minerals and Materials*, 2nd edn. Springer, Cham, Switzerland, xix + 606 pp., <https://doi.org/10.1007/978-3-319-24765-6>.
- Gaillou, E., Delaunay, A., Rondeau, B., Bouhnik-le-Coz, M., Fritsch, E., Cornen, G. & Monnier, C. 2008. The geochemistry of gem opals as evidence of their origin. *Ore Geology Reviews*, **34**(1–2), 113–126, <https://doi.org/10.1016/j.oregeorev.2007.07.004>.
- Han, X., Feng, X., Li, W. & Guo, S. 2020. One kind of new Ti³⁺ luminous center in Ti:Al₂O₃ crystals. *Optical Materials*, **105**, article 109881, <https://doi.org/10.1016/j.optmat.2020.109881>.
- Hu, X., Luo, W., Zang, D., Wang, W., Yi, C. & Li, J. 2023. Key factors affecting hydrocarbon accumulation in ancient dolomite gas reservoirs of Xixiangchi Formation (southern Sichuan basin, China). *Frontiers in Earth Science*, **10**, article 1022911, <https://doi.org/10.3389/feart.2022.1022911>.
- Jiang, Y., Gu, Y., Zhu, X., Xu, W., Xiao, Y. & Li, J. 2017. Hydrothermal dolomite reservoir facies in the Sinian Dengying Fm, central Sichuan basin. *Natural Gas Industry B*, **4**(4), 287–293, <https://doi.org/10.1016/j.ngib.2017.08.012>.
- Kiefer, C.L. 1953. Note sur quelques minéraux rares du groupe des phyllites. *Bulletin de la Société Française de Minéralogie et de Cristallographie*, **76**(1), 63–78, <https://doi.org/10.3406/bulmi.1953.4815>.
- Melchiorre, E.B., Criss, R.E. & Rose, T.P. 2000. Oxygen and carbon isotope study of natural and synthetic azurite. *Economic Geology*, **95**(3), 621–628, <https://doi.org/10.2113/gsecongeo.95.3.621>.
- Melka, K. 2009. A scheme for the classification of micaceous minerals. *Acta Geodynamica et Geomaterialia*, **6**(1), 69–75, https://www.irsm.cas.cz/materialy/acta_content/2009_01/4_Melka1.pdf.
- Mu, H., Yan, D., Qiu, L., Yang, W., Kong, R., Gong, L. & Li, S. 2019. Formation of the Late Triassic western Sichuan foreland basin of the Qinling orogenic belt, SW China: Sedimentary and geochronological constraints from the Xujiache Formation. *Journal of Asian Earth Sciences*, **183**, article 103938, <https://doi.org/10.1016/j.jseas.2019.103938>.
- Nespolo, M. 2001. Perturbative theory of mica polytypism. Role of the M2 layer in the formation of inhomogeneous polytypes. *Clays and Clay Minerals*, **49**(1), 1–23, <https://doi.org/10.1346/ccmn.2001.0490101>.
- Notari, F., Grobon, C. & Fritsch, E. 2002. Observation des émeraudes traitées en luminescence U-VISIO. *Revue de Gemmologie AFG*, No. 144, 27–31.
- Notari, F., Caplan, C., Hainschwang, T. & Nach, C. 2022. Les substances de remplissage des émeraudes. In: Giuliani, G. (ed) *Émeraudes, Tout un Monde!* Les Éditions du Piat, Paris, France, 295–302.
- Olivier, B. 2006. *The geology and petrology of the Merelani tanzanite deposit, NE Tanzania*. PhD thesis, University of Stellenbosch, South Africa, 434 pp.
- Petterd, W.F. 1910. *Catalogue of the Minerals of Tasmania*. Mines Department and John Vail, Government Printer, Hobart, Tasmania, Australia, 221 pp. (see p. 22), <https://books.google.com/books?id=bvVYAAAAYAAJ>.

- Pirouei, M., Kolo, K. & Kalaitzidis, S.P. 2020. Chromium-rich muscovite mineralization in Zagros ophiolites in Iraqi Kurdistan: A study on fuchsite paragenetic association with listvenite types. *Arabian Journal of Geosciences*, **13**(17), article 864, <https://doi.org/10.1007/s12517-020-05887-6>.
- Pradat, T., Rondeau, B. & Fritsch, E. 2013. Gem News International: Unusual faceted massive fuchsite. *Gems & Gemology*, **49**(3), 183–184.
- Reddy, S.L., Reddy, R.R.S., Reddy, G.S., Rao, P.S. & Reddy, B.J. 2003. Optical absorption and EPR spectra of fuchsite. *Spectrochimica Acta Part A: Molecular and Biomolecular Spectroscopy*, **59**(11), 2603–2609, [https://doi.org/10.1016/s1386-1425\(03\)00019-2](https://doi.org/10.1016/s1386-1425(03)00019-2).
- Rieder, M., Cavazzini, G., D'yakonov, Y.S., Frank-Kamenetskii, V.A., Gottardi, G., Guggenheim, S., Koval', P.W., Müller, G. *et al.* 1999. Nomenclature of the micas. *Mineralogical Magazine*, **63**(2), 267–279, <https://doi.org/10.1180/002646199548385>.
- Ryder, R.T., Rice, D.D., Zhaocai, S., Yigang, Z., Yunyu, Q. & Zhengwu, G. 1994. *Petroleum Geology of the Sichuan Basin, China – Report on U.S. Geological Survey and Chinese Ministry of Geology and Mineral Resources Field Investigations and Meetings, October 1991*. Report 2331-1258, U.S. Geological Survey, Washington DC, USA, 67 pp.
- Sambandam, B., Michael, R.J.V. & Manoharan, P.T. 2015. Oxygen vacancies and intense luminescence in manganese loaded ZnO microflowers for visible light water splitting. *Nanoscale*, **7**(33), 13935–13942, <https://doi.org/10.1039/c5nr02666k>.
- Summers, G.P., Wilson, T.M., Jeffries, B.T., Tohver, H.T., Chen, Y. & Abraham, M.M. 1983. Luminescence from oxygen vacancies in MgO crystals thermochemically reduced at high temperatures. *Physical Review B*, **27**(2), 1283–1291, <https://doi.org/10.1103/PhysRevB.27.1283>.
- Tappert, M.C., Rivard, B., Giles, D., Tappert, R. & Mauger, A. 2013. The mineral chemistry, near-infrared, and mid-infrared reflectance spectroscopy of phengite from the Olympic Dam IOCG deposit, South Australia. *Ore Geology Reviews*, **53**, 26–38, <https://doi.org/10.1016/j.oregeorev.2012.12.006>.
- Wang, J., Bao, C. & Guo, Z. 1989. Formation and development of the Sichuan basin. In: Zhu, X. (ed) *Chinese Sedimentary Basins*. Elsevier, Amsterdam, The Netherlands, 147–163.
- Wang, T.-S., Wang, G.-F., Qiu, M.-L., Cheng, W., Zhang, J.-F. & Zhao, G.-Q. 2021. The origin of the 500 nm luminescence band related to oxygen vacancies in ZrO₂. *Journal of Luminescence*, **237**, article 118133, <https://doi.org/10.1016/j.jlumin.2021.118133>.
- Whitmore, D.R.E., Berry, L.G. & Hawley, J.E. 1946. Chrome micas. *American Mineralogist*, **31**(1–2), 1–21.
- Wood, D. L. & Nassau, K. 1968. The characterization of beryl and emerald by visible and infrared absorption spectroscopy. *American Mineralogist*, **53**(5–6), 777–800.
- Yang, X., Huang, Z., Wang, X., Wang, Y., Li, K. & Zeng, D. 2019. Origin of crystal dolomite and its reservoir formation mechanism in the Xixiangchi Formation, Upper Cambrian in southeastern Sichuan basin. *Carbonates and Evaporites*, **34**(4), 1537–1549, <https://doi.org/10.1007/s13146-019-00499-y>.
- Zhang, C., Yu, X. & Jiang, T. 2019. Mineral association and graphite inclusions in nephrite jade from Liaoning, northeast China: Implications for metamorphic conditions and ore genesis. *Geoscience Frontiers*, **10**(2), 425–437, <https://doi.org/10.1016/j.gsf.2018.02.009>.
- Zheng, H., Ma, Y., Chi, G., Qing, H., Liu, B., Zhang, X., Shen, Y., Liu, J. *et al.* 2019. Stratigraphic and structural control on hydrothermal dolomitization in the Middle Permian carbonates, southwestern Sichuan basin (China). *Minerals*, **9**(1), article 32, <https://doi.org/10.3390/min9010032>.

The Authors

Dr Féodor Blumentritt¹, Franck Notari¹, Marion Becouze¹, Maxence Vigier², Guillaume Zuber¹, Candice Caplan FGA¹ and Dr Emmanuel Fritsch FGA²

¹ GGTL Laboratories Switzerland, 4bis route des Jeunes, 1229, Geneva, Switzerland

² University of Nantes, CNRS, Institut des Matériaux de Nantes Jean Rouxel, 44000 Nantes, France

Email: feodor.blumentritt@ggtl-lab.org

Acknowledgments

We warmly thank Dr Nicolas Meisser of the University of Lausanne, Switzerland, for fruitful advice on geological formation and help to support and confirm chemical and structural analyses. We thank Ms Phakamon Pokpoon (Bangkok, Thailand) for help cutting and polishing the cabochons. We also thank Clara Allriol-Mouton (GGTL Laboratories, Switzerland) for helpful cataloguing of the numerous samples.